Texture and Microstructure Development during Intercritical Rolling of Low-Carbon Steels

A. BODIN, J. SIETSMA, and S. VAN DER ZWAAG

Laboratory rolling trials have been performed to investigate the development of microstructure and crystallographic texture during and after intercritical rolling. The finishing temperature was varied over a wide range, and samples were taken just prior to the last pass, after quenching following the last pass, after air cooling and coiling, and after accelerated cooling and coiling. Cooling of the samples to the entry temperature for the last pass does not influence the texture of the sample, nor do higher cooling rates after austenitic finishing within the range of cooling rates in this study, although it may cause a refinement of the ferrite grains. Recrystallization after intercritical rolling leads to a decrease in texture intensity. In the case of recrystallization of low-carbon steels, the nucleation mechanism is strain-induced boundary migration (SIBM), which leads to unfavorable textures for deep drawing. In the case of recrystallization of interstitial-free (IF) steel after ferritic rolling, the nucleation mechanism shifts from the SIBM mechanism at high finishing temperatures to subgrain coalescence at (SGC) low finishing temperatures. The latter mechanism leads to more favorable textures for deep-drawing applications. Transformation-induced (TI) nucleation explains the occurrence of a sudden increase in ferrite grain size after high-temperature intercritical deformation of low-carbon (LC) steels.

I. INTRODUCTION

THE properties of a material depend heavily on the combination of grain size, morphology, and crystallographic texture. The texture is particularly important to the formability of the material, more specifically, to deep-drawing properties.[1] There is a clear relationship between the intensities of certain crystallographic orientations and, for instance, the deep-drawing ratio or the *r*-value.[1] The texture also has consequences for other mechanical properties. In particular, in high-strength low-alloy steels, a retained deformation texture may result in an increased strength of the steels by promoting a smaller ferrite grain size.[2] Furthermore, in the production of high-strength plate in a plate mill, the rolling of thinner gages often results in intercritical deformation. In addition to the texture that results from the deformed and subsequently partially transformed austenite, intercritical deformation increases the amount of texture formation upon further deformation of the two-phase structure.[3,4] In most cases, the formability in terms of *r*-value is irrelevant for these kinds of steels, but the difference in mechanical properties in the longitudinal and transverse directions is highly relevant.[4]

The changes in crystallographic orientation during deformation of grains are not random. They are a consequence of deformation occurring on the most favourably oriented slip or twinning systems. As a result, the deformed material acquires a preferred orientation or texture. If the metal subsequently recrystallizes, nucleation may occur preferentially in regions of a particular orientation.[5] The ability of the nucleus to grow is determined primarily by the orientations of adjacent regions in the microstructure. Together, these features (nucleation and growth) ensure that a texture also develops in the recrystallized material. Such a texture is called a recrystallization texture to distinguish it from the deformation texture from which it develops. In the case of deformation of austenite, the transformation of the deformed or recrystallized austenite into ferrite results in a transformation texture.[3] The relation between the orientation of the crystallites in the austenite and the resulting orientation in the ferrite can be described by an orientation relationship. In the case of the austenite-to-ferrite transformation, the Kurdjumov–Sachs orientation relationship is widely used and commonly accepted.[6] Transformation after rolling below the austenite recrystallization temperature (T_{nr}) results in a sharper austenite deformation texture than after recrystallization-controlled rolling (*i.e.*, above T_{nr}).[2] The suppression of the austenite recrystallization results in continued straining of the austenite (pancaking), thereby producing a sharp γ-rolling texture. As a result, a marked α-texture is produced after transformation. Intercritical rolling of steel complicates matters considerably, because the final texture will the result of the austenite recrystallization texture, the austenite deformation texture, the transformation texture, the ferrite deformation texture, and, finally, the ferrite recrystallization texture. Especially when the deformation is followed by a recrystallization treatment or by subsequent cold rolling and annealing, it is important to understand the texture development during and after hot rolling, since the final texture depends strongly on the texture of the hot-rolled strip.[7]

The development of the microstructure is also determined by the successive deformation and recrystallization processes. After each deformation step, the amount of deformation of the material, the deformation temperature, the strain rate, and the time after deformation determine whether the microstructure recrystallizes or recovers. The effect of work hardening and softening on the microstructural development

A. BODIN, Researcher, is with Corus Research, Development & Technology, IJmuiden Technology Centre, Steel Metallurgy, 1970 CA IJmuiden, The Netherlands. Contact e-mail: andre.bodin@corusgroup.com J. SIETSMA, Associate Professor, and S. VAN DER ZWAAG, Professor, are with the Laboratory of Materials Science, Delft University of Technology, 2628 AL Delft, The Netherlands.

Manuscript submitted August 14, 2000.

of single-phase steels (either austenitically or ferritically deformed) has been the subject of many studies.[8] The effect of work hardening and softening of intercritically deformed steels on the microstructural development has not been as widely studied.

To study the effect of intercritical deformation on the development of microstructure and texture of steels, a detailed investigation was made. As the metallurgical processes involved depend heavily on the chemical composition as well as on the thermomechanical treatment, the study considered four low-carbon (LC) steels with different chemical compositions. The experimental results will be explained in terms of their relation to the chemical composition of the materials and to the different ratios of phase constituents during hot deformation.

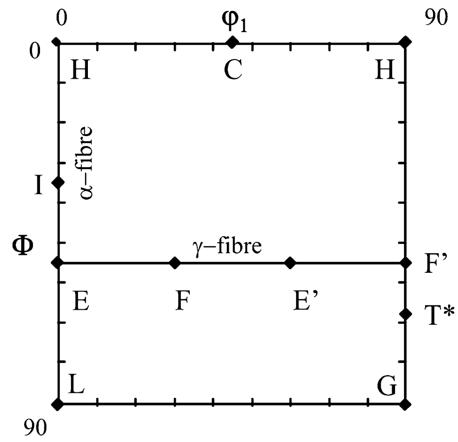

Fig. 1—Location of important texture components in the φ_2 = 45 deg section of the ODF.

II. TEXTURE DEVELOPMENT DURING HOT ROLLING AND DIRECT ANNEALING

A. *General*

Plastic deformation of a polycrystalline material results in a predominance of a particular crystallographic direction or plane parallel to the direction of deformation in a majority of individual crystals comprising the material.[6] In a tensile test on a single crystal, the slip direction rotates until it approaches the axis of tension, and in compression, the slip direction rotates until it approaches the plane of compression. Similarly, rotations occur in the individual grains of a polycrystalline material. In this case, the grains undergo more complicated stressing even in simple processes such as tension or compression; this leads to the development of preferred orientations or texture, the degree and nature of which depend on the particular deformation process as well as on the crystal structure of the metal. Texture may also result from recrystallization or phase transformation: in both cases, new grains are formed which have specific orientations with respect to the parent grains.

B. *Representation of Texture*

Textures are usually presented in the form of an orientation distribution function (ODF). This is a representation of the texture, which is calculated from individual pole figures for low-index planes. The orientation of an individual crystallite can be specified by considering its crystal coordinate system (x', y', and z'), with the axes being the axes of the cubic unit cell, with respect to a common sample coordinate system (x, y, and z). These coordinate systems are related to each other by the Euler angles φ_1, Φ, and φ_2. The ODF for the orientation **g** can then be defined as the density of crystallites with the orientation **g**. The ODF can be represented either by a perspective drawing of the Euler space or by a two-dimensional representation of cross-sectional planes. The intensity of an orientation is expressed with respect to the intensity this orientation would have had in a sample with a completely random texture.

Apart from allowing a more quantitative description of textures than is possible using pole figures, the use of the ODF allows the identification of texture fibers and quantitative plots of intensity along these fibers. These intensity data provide detailed information. The volume fractions of any texture component may also be readily calculated from the ODF.[9] Such simple yet quantitative representations of the data may be compared directly with theoretical predictions or may form part of the specification of an industrial product because, based on the ODF, theoretical r-values can be calculated.[10]

The part of the ODF shown in Figure 1 (defined by φ_2 = 45 deg) contains most of the relevant texture components and fibers for a bcc metal.[2] The most important fibers are the α-fiber and the γ-fiber. The α-fiber is the collection of orientations with the $\langle 110 \rangle$ direction parallel to the rolling direction, and the γ-fiber is the collection of orientations with the $\{111\}$ plane parallel to the rolling plane. In bcc metals, a dominant orientation is $\{001\}\langle 110 \rangle$ with cube planes in the rolling planes and the $\langle 110 \rangle$ direction in the rolling direction (letter H in Figure 1), but there are other important components such as $\{112\}\langle 110 \rangle$ (letter I), $\{111\}\langle 110 \rangle$ (letter E), and $\{111\}\langle 112 \rangle$ (letter F).

C. *Texture Development in Austenite*

The deformation of fcc metals such as austenite occurs by slip or by twinning. The preferred slip system is always the same: the close-packed plane $\{111\}$ slips in the close-packed direction $\langle 110 \rangle$ and twinning occurs at the $\{111\}\langle 112 \rangle$ system.[6] Austenite has a predominant $\{110\}\langle 112 \rangle$ rolling texture with a $\{110\}$ plane in the rolling plane and a $\langle 112 \rangle$ direction in the rolling direction (usually referred to as "brass texture").[3] A second component which is important in the rolling texture is the $\{112\}\langle 111 \rangle$ component ("copper texture"). The S component, $\{123\}\langle 634 \rangle$, is also reported to be an important component in the austenite deformation texture.[3] The Goss component $\{110\}\langle 001 \rangle$ is a minor deformation component.[11]

When a metal is deformed at a high temperature, the deformed microstructure usually recovers or recrystallizes. The influence of recovery on the texture development is indirect, because recovery leads to a rapid polygonization of grains on the γ-fiber, in contrast to α-fiber, orientations.[12] This polygonization allows stable recrystallization nuclei to form. The grains with orientations on the α-fiber are consumed and, thus, the intensity of the γ-fiber components is enhanced as a result of recovery-stimulated nucleation of recrystallization.[12] The recrystallized structure possesses a preferred orientation which, in many cases, is stronger than in the deformed structure. This recrystallization texture results from primary recrystallization of the deformed grains, or from growth of selected grains in the recrystallized material (secondary recrystallization). The main recrystallization texture component in austenite is the cube component $\{100\}\langle 001\rangle$.[3] The magnitude of the influence of this component in the final texture depends largely on the degree of recrystallization in austenite and, hence, on the temperature at which the deformation takes place with respect to the nonrecrystallization temperature (T_{nr}). At higher temperatures, the austenite will recrystallize and the cube texture will be formed. At deformation temperatures below T_{nr}, the austenite will not recrystallize and a sharper deformation texture may develop by subsequent deformation.[2]

D. *Transformation Texture*

If the austenite possesses a crystallographic texture, the ferrite that forms from the austenite upon cooling will also acquire a texture which can be related to the texture of the austenite by means of an orientation relationship. In general, orientation relationships are expressed as

$$\{h_1k_1l_1\}\|\{h_2k_2l_2\} \cap \langle u_1v_1w_1\rangle\|\langle u_2v_2w_2\rangle \qquad [1]$$

where subscripts 1 and 2 refer to the parent and product structures of the phase transformation, respectively. In the case of steels, three orientation relationships are usually distinguished: the Bain orientation relation, the Kurdjumov–Sachs orientation relation, and the Nishiyama–Wasserman orientation relation.[3] Experimental evidence indicates that the Kurdjumov–Sachs orientation relationship can be used to describe the transformation from ferrite to austenite.[6,13,14] The rotation axis in this case is the $\langle 112\rangle$ direction, and transformation is the result of a rotation of 90 deg around that axis. A $\{111\}$ plane in the austenite phase transforms into a $\{011\}$ plane in the ferrite, and a $\{011\}$ plane in the austenite transforms into a $\{111\}$ plane in the ferrite. As a result of crystallographic symmetry, a number of equivalent orientations are possible. It appears that the transformation of austenite to ferrite involves only a restricted set of the 24 possible K-S variants. This phenomenon is known as variant selection, and its origins have been investigated by many authors.[3,11] As a result of the phase transformation, the $\{110\}\langle 112\rangle_\gamma$ rolling-texture component will transform into the $\{332\}\langle 113\rangle_\alpha$ component (T*), and the $\{112\}\langle 111\rangle_\gamma$ rolling-texture component will transform into the $\{113\}\langle 110\rangle_\alpha$ component in the ferrite. The cube texture from recrystallized austenite will result in a $\{100\}\langle 110\rangle_\alpha$ component, in a $\{110\}\langle 001\rangle_\alpha$ Goss component, or in the $\{110\}\langle 110\rangle_\alpha$ rotated Goss component (L). The S component transforms into the $\{332\}\langle 113\rangle_\alpha$ component, the $\{113\}\langle 110\rangle_\alpha$ component, and the rotated Goss component. The Goss deformation component is a minor component and will not be considered in the remainder of this article. These transformations are summarized in the first two columns of Table I.

E. *Texture Development during Intercritical Rolling*

In ferrite, with its bcc structure, no close-packed planes exist. The close-packed direction is the $\langle 111\rangle$ direction, and the plane with the highest density is the $\{110\}$ plane. Apart from the $\{110\}\langle 111\rangle$ slip system, the $\{112\}\langle 111\rangle$ and the $\{123\}\langle 111\rangle$ slip systems can also be activated.[6]

The inheritance of a texture by ferrite from austenite depends mainly on the strength of the rolling texture of the parent austenite. The deformation and subsequent cooling of an austenite-ferrite two-phase structure leads to

(1) crystal rotation by further deformation of the remaining austenite phase;
(2) (possibly) recrystallization of the austenite;
(3) crystal rotation by deformation of the ferrite phase to more stable texture components;
(4) (possibly) recrystallization of the ferrite; and
(5) completion of the austenite-to-ferrite transformation.

The deformation of the austenite in the two-phase structure will not result in new texture components, neither during recrystallization of the austenite nor during transformation into ferrite. Compared to fully austenitic rolling, the texture components $\{112\}\langle 111\rangle_\gamma$ and $\{110\}\langle 112\rangle_\gamma$ will intensify as a result of deformation at a lower temperature.[2] Deformation of the ferrite does result in texture modifications. The ferrite grains rotate as a result of the deformation and the $\{113\}\langle 110\rangle_\alpha$ texture component changes into the stable component $\{112\}\langle 110\rangle_\alpha$ (rotation of 10 deg around the rolling direction//$\langle 110\rangle$), and the $\{332\}\langle 113\rangle_\alpha$ component changes into $\{111\}\langle 110\rangle_\alpha$ via the intermediate stages $\{554\}\langle 225\rangle_\alpha$ and $\{111\}\langle 112\rangle_\alpha$ (rotation of 4, 14, and 44 deg around the transverse direction//$\langle 110\rangle$). These rotations are summarized in Table I. Deformation of the ferrite after transformation only affects the intensity of the texture components that were already present after intercritical rolling. The increase in rotation of the grains and the increase in dislocation density are both important factors in stimulating recrystallization.

F. *Texture Development by Recrystallization of Ferrite*

Dillamore reported that in case of deformation of ferrite, the stored energy in the grains increases in the sequence $\{001\}\langle 110\rangle_\alpha \leq \{112\}\langle 110\rangle_\alpha \leq \{111\}\langle 110\rangle_\alpha \leq \{110\}\langle 110\rangle_\alpha$.[15] The stored energy has a considerable influence on the annealing texture. Nucleation by subgrain coalescence (SGC) within individual deformed grains is facilitated if the stored energy of the grains is large, and this favors formation of textures with $\{111\}\langle 110\rangle_\alpha$ and $\{110\}\langle 110\rangle_\alpha$ orientations. Another recrystallization nucleation mechanism, strain-induced boundary migration (SIBM), is based on bulging of a preexisting grain boundary into grains of high stored energy.

This implies nucleation inside grains with a low stored energy, *i.e.*, $\{001\}\langle 110\rangle_\alpha$ and $\{112\}\langle 110\rangle_\alpha$ grains. If recrystallization nucleates near hard second-phase particles like cementite, the texture development has a more random character.[17]

III. EXPERIMENTAL

A. *Material*

The steels were taken from commercially produced semi-finished slabs with a thickness of 37 mm. Table II shows the chemical composition of the steels. The interstitial-free (IF) steel contains a very low carbon content and no free

Table I. Origin and Evolution of Some Characteristic Texture Components during Austenitic, Intercritical, or Ferritic Rolling of Steel[3]

Texture Components in Austenite		Transformation Kurdjumov–Sachs		Rotation around RD or TD// $\langle 110 \rangle$ as Result of Intercritical Deformation	Orientation (*cf.* Figure 1)	φ_1, Φ, φ_2
$\{110\}\ \langle 112 \rangle_\gamma$ (deformation, brass)	$\rightarrow$	$\{332\}\ \langle 113 \rangle_\alpha$	$\rightarrow$	4 deg about TD $\{554\}\ \langle 225 \rangle_\alpha$	T*	90, 60, 45
			$\rightarrow$	10 deg about TD $\{111\}\ \langle 112 \rangle_\alpha$	γ-fibr (F)	90, 55, 45
$\{112\}\ \langle 111 \rangle_\gamma$ (deformation, copper)	$\rightarrow$	$\{113\}\ \langle 110 \rangle_\alpha$	$\rightarrow$	10 deg about RD $\{112\}\ \langle 110 \rangle_\alpha$	I	0, 35, 45
			$\rightarrow$	24 deg about RD $\{445\}\ \langle 110 \rangle_\alpha$	α-fiber	0, 48, 45
			$\rightarrow$	30 deg about RD $\{111\}\ \langle 110 \rangle_\alpha$	γ-fibr (E)	0, 55, 45
$\{123\}\ \langle 634 \rangle_\gamma$ (deformation, S)	$\rightarrow$	$\{113\}\ \langle 110 \rangle_\alpha$		see above	I, α-fiber, E	
	$\rightarrow$	$\{332\}\ \langle 113 \rangle_\alpha$		see above	T*, γ-fibr, I	
	$\rightarrow$	$\{110\}\ \langle 110 \rangle_\alpha$		see above	L	
$\{100\}\ \langle 001 \rangle_\gamma$ (recrystallization)	$\rightarrow$	$\{100\}\ \langle 011 \rangle_\alpha$		—	H	0, 0, 45
	$\rightarrow$	$\{110\}\ \langle 001 \rangle_\alpha$		—	Goss	90, 90, 45
	$\rightarrow$	$\{110\}\ \langle 110 \rangle_\alpha$		—	L	0, 90, 45

Table II. Chemical Composition of the Steels (in Weight Percent or Parts per Million (N))

Code	C	Mn	Si	P	S	Al	Ti	N
IF	0.002	0.150	0.008	0.009	0.007	0.033	0.044	25
ELC	0.019	0.187	0.008	0.009	0.010	0.044	—	25
LC	0.052	0.230	0.004	0.010	0.012	0.052	—	26
CMn	0.103	0.490	0.006	0.010	0.014	0.035	—	45

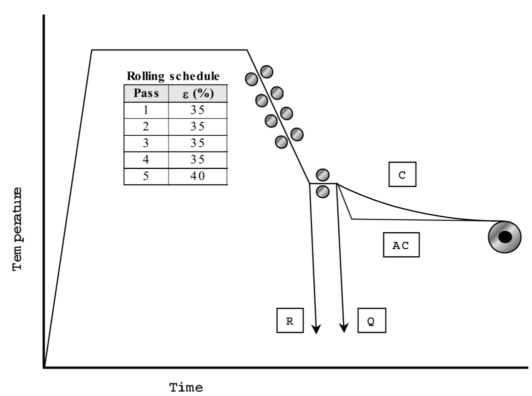

Fig. 2—Experimental rolling and temperature schedule.

nitrogen as a result of the titanium addition. The extralow carbon (ELC) and LC steels have nearly identical chemical compositions, apart from the carbon content. The differences in manganese content can be neglected. The carbon-manganese (CMn) steel contains twice the level of carbon and manganese in comparison to the LC steel. Apart from the carbon and manganese levels and the titanium in the IF steel, the chemical compositions of all steels are comparable. The transfer bars were cut into laboratory rolling samples measuring $100 \times 150 \times 37$ mm^3 (width $\times$ length $\times$ height).

B. *Laboratory Hot-Rolling Trials*

The samples were reheated at 1250 °C for 30 minutes and rolled on a laboratory mill (work roll diameter of 230 mm) in four passes, with reductions of 35 pct each from 37 to 6.3 mm (Figure 2). The entry temperatures for the first four passes were 1050 °C, 1020 °C, 985 °C (1000 °C), and 950 °C (975 °C), respectively (in parentheses are the required entry temperatures for the third and fourth passes, to achieve the finishing temperature of 950 °C). The final pass of 40 pct to 4 mm was performed at temperatures between 950 °C and 650 °C (Table III). The rolling passes were performed without work-roll lubrication. After finishing, the material was water quenched immediately after rolling (schedule Q, cooling rate ~50 °C/s), or it was allowed to cool to the coiling temperature in still air (schedule C, cooling rate ~1 °C/s). The coiling simulation was performed in a computer-controlled furnace (cooling rate ~1 °C/min). These specimens represent the hot-rolled and coiled material, whereas the quenched samples represent the "full-hard" microstructure. Schedule R allows the determination of the structure and texture of the material just prior to the final rolling pass. The influence of accelerated cooling on the texture development was determined by cooling austenitically finished samples on the laboratory run-out table at 40 °C/s (schedule AC).

The finish rolling temperature was measured by means of an infrared pyrometer. A reference rolling experiment, with thermocouples inserted in the center of the sample, showed that the maximum difference between the surface temperature and the center just prior to the final rolling pass is less than 10 °C. The deformation temperatures given throughout this article are the measured surface temperatures.

C. *Equilibrium Fractions*

To enable a quantitative evaluation of the behavior of intercritically deformed steels, the equilibrium fractions of austenite and ferrite as a function of temperature and chemical composition were calculated using MTDATA* (using the SGTE database). Since redistribution of manganese, a substitutional element, is assumed to be slow, the "paraequilibrium" state is considered. On the basis of the MTDATA calculations, the following expression for the molar fraction of carbon in austenite in the two-phase region of a psuedobinary "Fe-C" diagram at a given Mn concentration x_{Mn} could be derived:[16]

*MTDATA is a trademark of National Physical Laboratory, Teddington, United Kingdom.

Table III. Rolling and Coiling Temperatures Used During the Experiments

Code	$T_{finishing}$ (°C) (Schedule AC)	$T_{finishing}$ (°C) (Schedules, C and Q)	$T_{quenching}$ (°C) (Schedule R)	$T_{coiling}$ (°C) (AC and C)
IF	950	950, 900, 875… 650	950, 900… 700	750
ELC	950	950, 900, 875… 650	950, 900… 700	680
LC	900	950, 900, 875… 650	900, 850… 700	680
CMn	900	950, 900, 875… 650	900, 850… 700	650

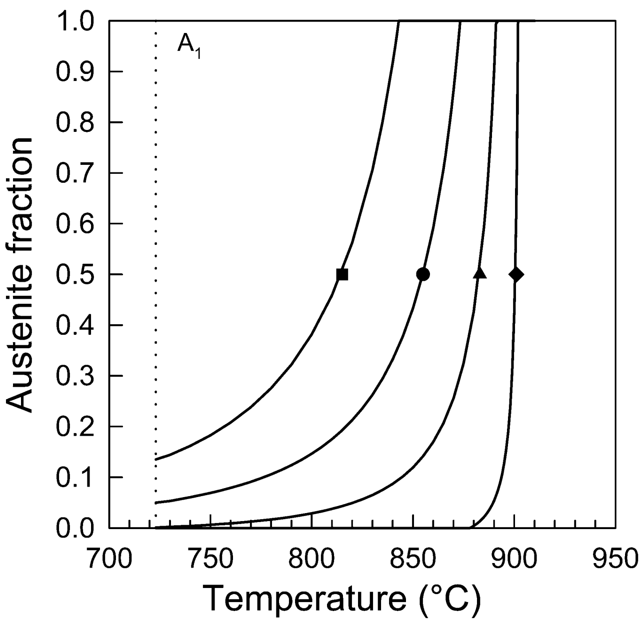

Fig. 3—Equilibrium fractions of austenite (γ) as a function of temperature for each of the steel grades (♦: IF; ▲: ELC; ●: LC; and ■: CMn).

$$x_C^\gamma = 0.951 + 0.126 \cdot x_{Mn} - (1.536 \cdot 10^{-3}\ K^{-1} + 2.766 \cdot 10^{-4}\ K^{-1} \cdot x_{Mn}) \cdot T + (6.188 \cdot 10^{-7}\ K^{-2} + 1.419 \cdot 10^{-7}\ K^{-2} \cdot x_{Mn}) \cdot T^2 \quad [2]$$

in which x_A^i is the molar fraction of element A in phase i (note that due to the paraequilibrium assumption $x_{Mn}{}^\gamma = x_{Mn}{}^\alpha = x_{Mn}$), and T is the temperature (in Kelvin). Similarly, the molar fraction of carbon in ferrite ($x_C{}^\alpha$) in the two-phase region can be given as[16]

$$x_C^\alpha = 5.532 \cdot 10^{-3} - 3.138 \cdot 10^{-4} \cdot x_{Mn} - (4.651 \cdot 10^{-6}\ K^{-1} - 5.340 \cdot 10^{-8}\ K^{-1} \cdot x_{Mn}) \cdot T \quad [3]$$

The ferrite and austenite fractions (f_α and f_γ respectively) can be calculated using

$$f_\gamma = \left(\frac{x_C^\alpha - x_C^0}{x_C^\alpha - x_C^\gamma}\right) \quad [4]$$

$$f_\alpha = \left(\frac{x_C^0 - x_C^\gamma}{x_C^\alpha - x_C^\gamma}\right) \quad [5]$$

in which $x_C{}^0$ is the overall carbon content of the alloy. With these equations, the equilibrium fractions of ferrite and austenite as a function of carbon and manganese content and temperature were calculated (Figure 3). The hardenability of the steels in this study is insufficient to determine the fraction of transformed austenite from the quenched microstructure by measuring the martensite content. To validate Eqs. [4] and [5], specimens of a steel with a higher carbon and manganese content were annealed at different temperatures in the intercritical region until equilibrium was reached. The specimens were then quenched and the fraction of martensite was determined. The agreement between the calculated and the measured fractions proved to be within the experimental errors. As a further check, the transformation temperatures were determined using a Bähr 805A/D plasto-dilatometer. The comparison of the calculated equilibrium transformation temperatures with the measured ones showed a good correspondence between measurements and calculations.

D. *Texture Measurements and Metallography*

The friction between the work rolls and the strip results in shear deformation of the surface. This results in a shear deformation texture, characterized by {110} components, and a compressive deformation texture in the center of the strip. This texture gradient persists after recrystallization of the hot-rolled strip and even after cold rolling and annealing. To eliminate the surface effects in the laboratory experiments, the texture is measured in the center of the material. The surface layer of the specimens is first removed by mechanical grinding and polishing and finally by electropolishing. The {110}, {200}, {211}, and {310} pole figures were measured using Co K_α radiation in a Siemens D5000 texture-goniometer. The ODF was calculated from these pole figures using the procedure developed by Van Houtte.[9] To enable comparison between the texture and the microstructure, the latter was also determined in the center of the sample using standard metallographical techniques.

E. *The Calculation of* r *Values*

Calculations based on the full-constraints (FC) Taylor model were applied to the texture measurements to predict the r-values of the material. Van Bael *et al.*[18] indicate that the FC model is relatively accurate in predicting the correct position of the ears for an IF steel in a cupping test, whereas the relaxed-constraints models would yield erroneous predictions. Van Houtte also concludes that the classical Taylor theory is a reliable qualitative model for the prediction of a wide range of deformation textures, although he emphasizes that more sophisticated models could provide more precise texture predictions.[18] In view of the qualitative nature of this study, the FC model is used to predict the r-values from the texture data. As a result of the chosen experimental procedure, only r-values parallel to rolling direction (denoted by r_0) were measured.

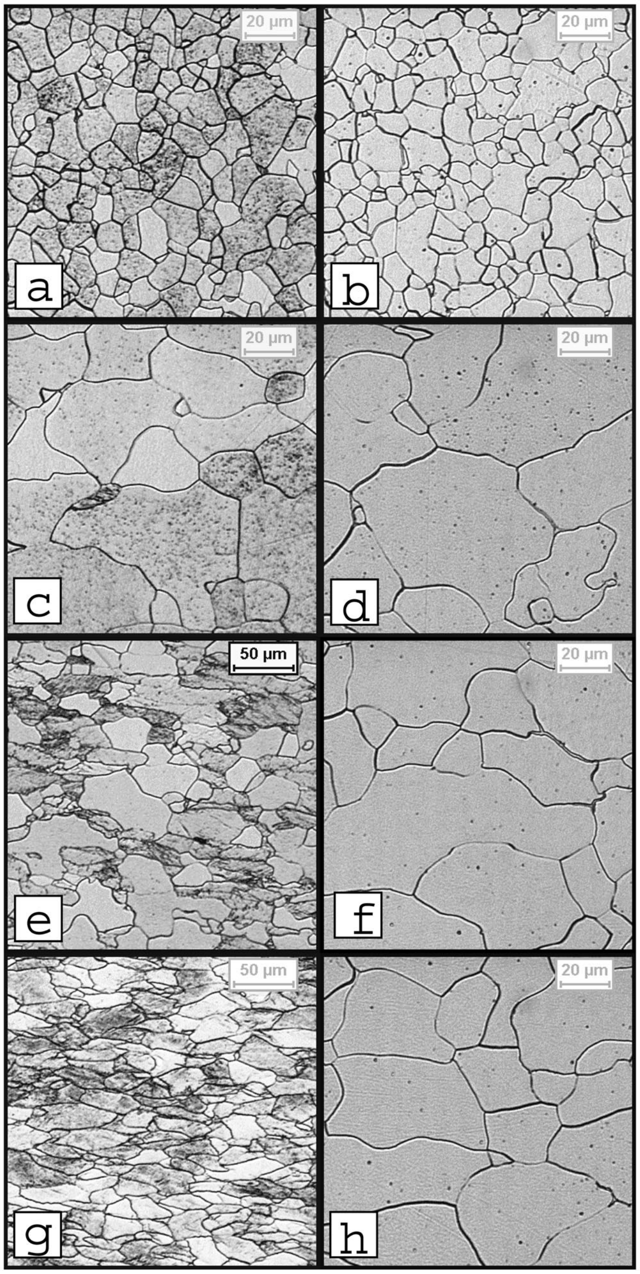

Fig. 4—Microstructures of ELC steel finished at 875 °C, (*a*) schedules Q and (*b*) C finished at 825 °C, schedules (*c*) Q and (*d*) C finished at 775 °C, schedules (*e*) Q and (*f*) C and finished at 725 °C, schedules (*g*) Q and (*h*) C.

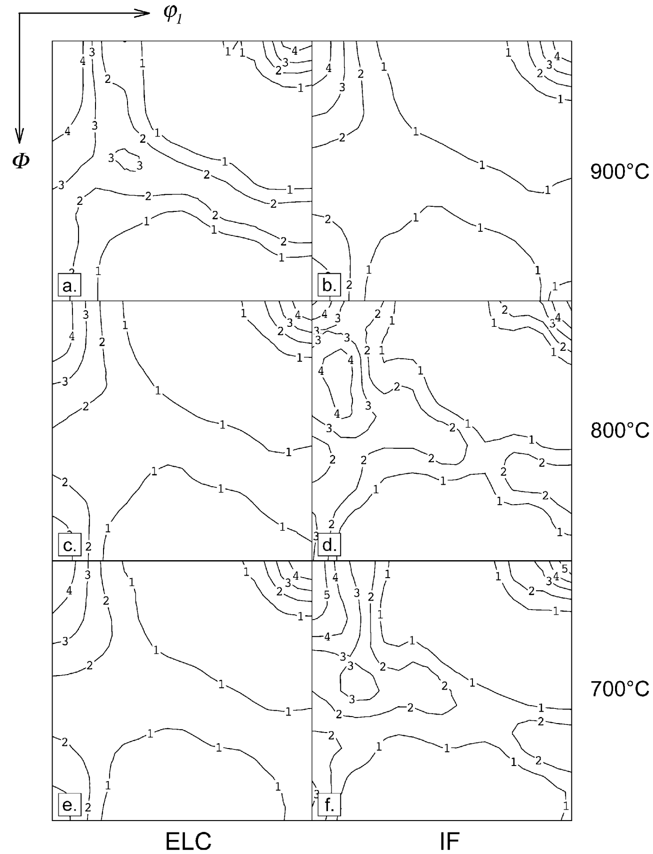

Fig. 5—Textures of the (*a*), (*c*), and (*e*) ELC steel and (*b*), (*d*), and (*f*) IF steel processed according to schedule R with a finishing temperature of 900 °C (a and b), 800 °C (c and d) and 700 °C (e and f) (φ_2 = 45 deg section of the ODF, and intensity levels: 1, 2, 3, . . .).

IV. RESULTS

The results of the metallographic and texture experiments are grouped by material. The behavior of the ELC steel is described in detail. For the other steel grades, the differences in behavior with respect to the ELC grade are reported.

A. *Microstructure of the ELC steel*

Austenitic finishing of the ELC steel, followed by quenching or coiling, results in a polygonal ferrite structure (average grain size of 14 μm) (Figure 4a). Reducing the finishing temperature to just above Ar_3 results in a finer grain size (12 μm). Accelerated cooling after austenitic finishing does not reduce the grain size further for IF and ELC steels. In case of the LC and CMn steels, the accelerated cooling does reduce the average grain size in comparison to the slow cooling (for LC steel, from 10 to 8 μm; for CMn steel, from 10 to 7 μm).

The sample finished at 875 °C, *i.e.*, at the high intercritical range, shows traces of a bimodal grain-size distribution. Small grains are located next to larger grains (Figure 4a). The sample finished at 850 °C shows the characteristic large ferrite grain size that is usually associated with ferritic rolling. As can be seen from the samples finished at lower temperatures, the recrystallized ferrite microstructure does not change as a result of lower rolling temperatures. The quenched microstructures show considerable changes. At 875 °C, the microstructure is polygonal and the grain size is small. The bimodal grain-size distribution can be observed in the quenched sample as well (Figure 4b). Finishing and quenching at 825 °C results in the same coarse ferrite grain as in the coiled sample, with a small amount of deformed ferrite still present (Figure 4c). Obviously, the recrystallization of the deformed ferrite proceeds very rapidly. A further reduction in finishing temperature results in an increased fraction of deformed ferrite in the quenched structure (Figures 4e and f). Only at a finishing temperature of 750 °C and below, which can be defined as low-temperature intercritical and ferritic rolling, the microstructure shows a completely strained ferrite which has completely recrystallized after coiling (Figures 4g and h).

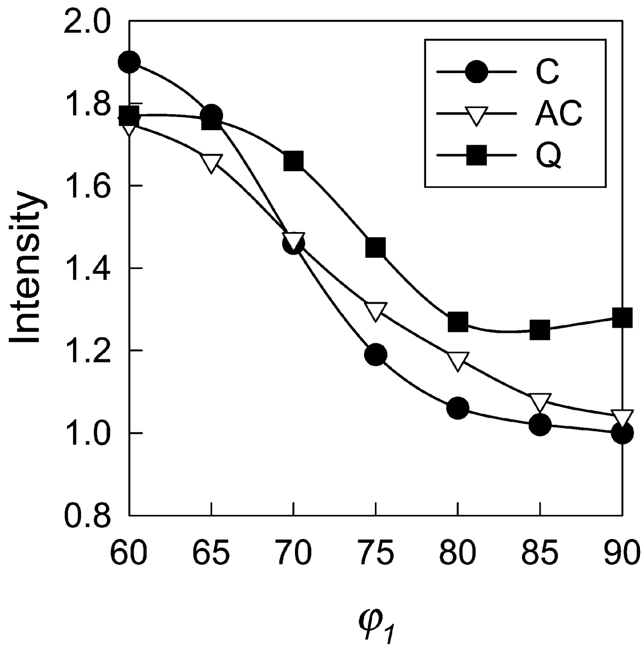

Fig. 6—Intensities along the partial γ-fiber for the ELC steel after quenching (schedule Q), after accelerated cooling and coiling (schedule AC), and after air cooling and coiling (schedule C).

B. *Texture of the ELC steel*

The textures that were determined after quenching before finish rolling (schedule R) indicate that there is no influence of the cooling process toward the final rolling pass on the texture. All textures show a high volume fraction of the austenite recrystallization and deformation components (H and I). A light deformation texture is visible in a faint and tilted γ-fiber (Figure 5). Austenitic deformation followed by transformation from austenite to ferrite sharpens the texture in comparison to the texture that was obtained by quenching before finishing. The cooling rate after finish rolling to the coiling temperature does not significantly change the texture (Figure 6), neither when cooled to 710 °C with different cooling rates (schedules AC and C), nor when quenched to room temperature (schedule Q).

Intercritical rolling at high temperatures results in an extension of the H-component along the α-fiber and, from deformation temperatures of 775 °C and lower, a clear γ-fiber starts to develop (Figure 7). However, the intensities of the components on the γ-fiber are never of the same magnitude as on the α-fiber. In Figure 8a, the ratio of the volume fraction of grains on the α-fiber and the γ-fiber after coiling and quenching is plotted as a function of deformation temperature. This figure indicates that at finishing temperatures of 750 °C and lower, the volume fraction of grains on the γ-fiber after quenching is lower than after recrystallization, and that the volume fraction of grains on the α-fiber shows a small reduction as a result of the recrystallization. Comparing schedule Q with schedule C for the components H, I, and E (Figures 8a) reveals that finish rolling at low temperatures (below 825 °C), followed by coiling, leads to an increase of the volume fraction of all three components. Since the volume fraction of grains on the α-fiber remains fairly constant, this means that specific orientations on the α-fiber increase, while at the same time others decrease.

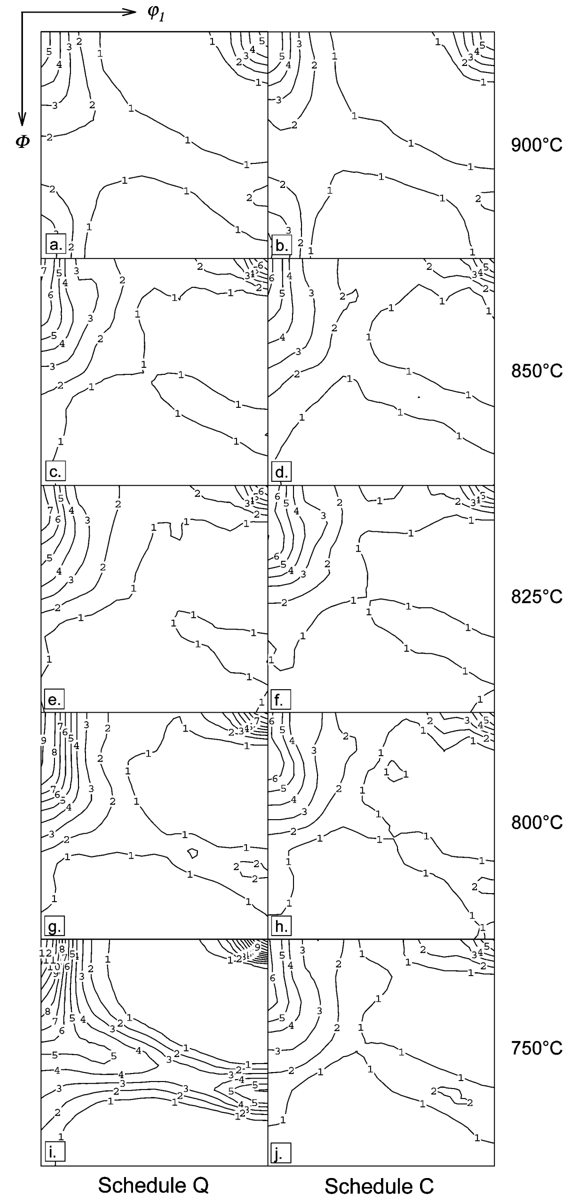

Fig. 7—Textures of the ELC steel before (schedule Q) and after (schedule C) coiling with a finishing temperature of 900 °C, (*a*) and (*b*) (*c*) and (*d*) 850 °C, (*e*) and (*f*) 825 °C, (*g*) and (*h*) 800 °C, and (*i*) and (*j*) 750 °C (φ_2 = 45 deg section of the ODF, and intensity levels: 1, 2, 3, . . .).

After finishing in the high intercritical region (between 875 °C and 800 °C), the volume fractions of α- and γ-fibers are unaffected by recrystallization. In comparison to the austenitically rolled specimens, the texture increase along the cube fiber ({100} ⟨uvw⟩) is notable (*e.g.*, Figure 7c). The intensities on the γ-fiber are very low (below the random value) after finishing, as well as after recrystallization.

Finish rolling in the ferrite region does not lead to textures different from those obtained by finishing in the low intercritical region.

In Figure 9, the r_0 values that were calculated based on the ODF data (schedules Q and C), as well as the measured values (schedule C only), are given for the ELC steel as well as the other steel grades. The influence of intercritical rolling seems to be more pronounced in the calculated values

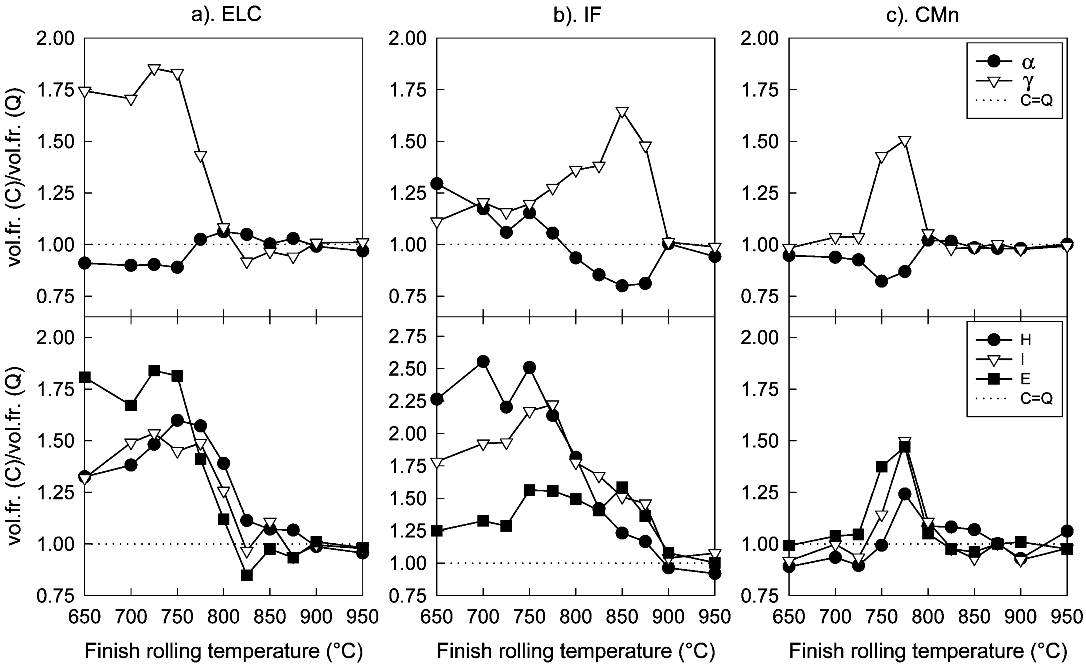

Fig. 8—Ratio of volume fractions of grains on the α-fiber and γ-fiber after (C) and before coiling (Q) as a function of finish rolling temperature ((*a*) ELC, (*b*) IF, and (*c*) CMn). Ratio of volume fractions of grains of the H, I, and E orientation after (C) and before coiling (Q) as a function of finish rolling temperature.

(which are based on the midplane texture) than in the measured values (which are based on the average texture over the thickness). Calculated Δr-values are given for schedule C.

C. *The IF Steel*

A large difference between the microstructures of the IF and the ELC steels is visible in the quenched samples. Due to the slow recrystallization behavior of the IF steel, the recrystallization is incomplete as soon as the microstructure starts to be partly ferritic. After finishing at 875 °C followed by immediate quenching, almost no recrystallized ferrite grains are visible (Figure 10), whereas the ELC steel showed a completely recrystallized microstructure down to deformation temperatures of 825 °C (Figure 4c).

The differences between the ELC and IF steels in the quenched microstructure are reflected in the texture (refer also to Figures 5 and 8). The texture of the IF specimen, finished at 875 °C, shows a deformation texture with a sharp α-fiber and a clear γ-fiber (Figure 11b). The maximum intensity is located near the I component. Another difference in the ELC steel is that the intensity of the texture seems to decrease with decreasing deformation temperature. A striking difference is the presence of a maximum intensity in the recrystallized samples after rolling at 775 °C or lower near the F component or, rather, the T* component (Figure 11h). This type of texture was not observed in the ELC steel (Figure 11g). The texture in the nonrecrystallized IF samples strongly resembles the ELC ones, the only differences being the stronger alignment of the γ-fiber along the $\Phi = 55$ deg line and the lower ratio of the volume fractions of grains on the α-fiber and the γ-fiber.

D. *The LC Steel*

The microstructural development of the LC steel is similar to that of the ELC steel. The only difference is the cementite morphology. The cementite morphology shows that deformation at 850 °C leads to cementite particles being oriented in all directions (Figure 12a), whereas deformation at 825 °C causes the cementite to align in the rolling direction (Figure 12b). Deformation at 700 °C can be defined as fully ferritic finishing, and it causes either large recrystallized grains after coiling or heavily deformed ferrite grains after quenching. In the recrystallized structure, the cementite is distributed very finely through the microstructure along the former deformed ferrite grains or the present recrystallized ones (Figure 12c). Also, some elongated cementite clusters are visible in the microstructure.

Apart from much higher maximum intensities in both the quenched and recrystallized samples, the general picture of the texture for the LC steel is very similar to that for the ELC steel texture.

E. *The CMn Steel*

Apart from a higher pearlite fraction, the microstructures of the austenitically finished CMn samples are similar to the LC ones (Figures 13a and b). Finishing in the high-temperature range of the intercritical region results in a bimodal grain-size distribution. This is particularly pronounced when finishing at 800 °C (Figures 13c and d). Finishing at 775 °C causes a very large grain size to occur after coiling, with traces of unrecrystallized ferrite in the microstructure (Figures 13e and f). After fully ferritic finishing ($T \leq 725$ °C), the microstructure remains elongated and does not recrystallize after finishing. The microstructures of the samples quenched after rolling reveal that the microstructure is mainly polygonal down to finishing temperatures of 825 °C. At a deformation temperature of 800 °C, the microstructure shows both recrystallized ferrite grains, deformed ferrite grains, and martensite. Finishing at 775 °C and lower shows a completely strained ferrite along with

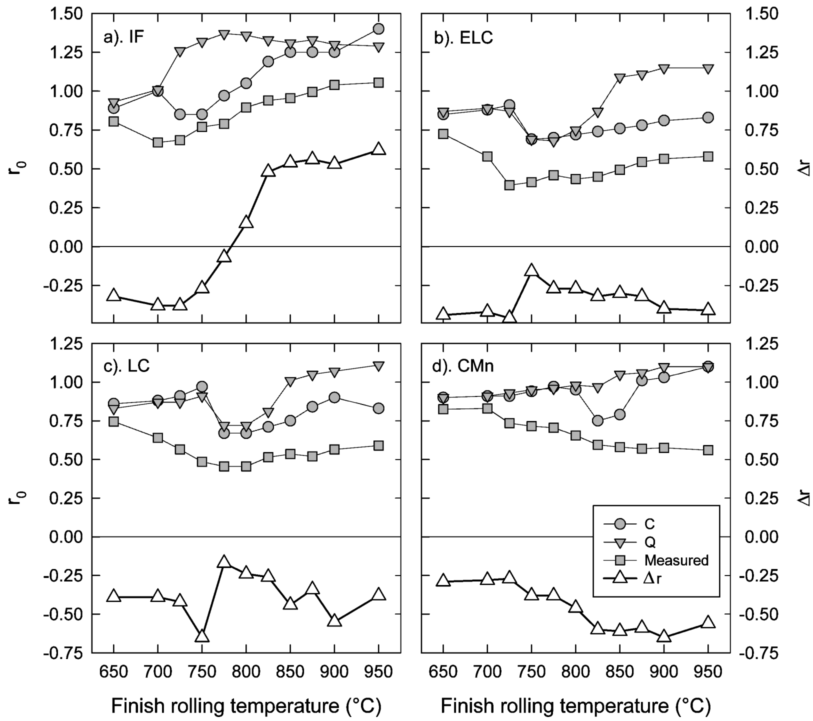

Fig. 9—Calculated r_0 values and Δr-values based on the full-constraint Taylor model and measured r_0 values as a function of finishing temperature for (*a*) IF steel, (*b*) ELC steel, (*c*) LC steel, and (*d*) CMn steel.

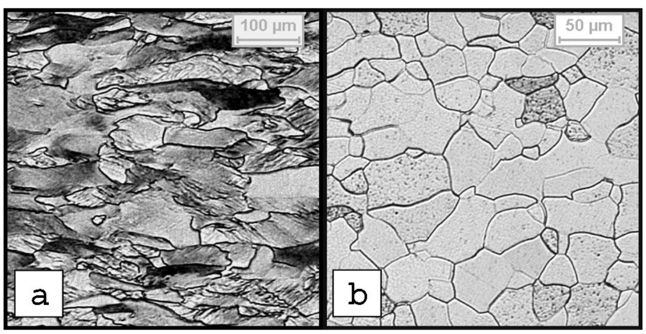

Fig. 10—Microstructures of IF steel finished at 875 °C, schedules (*a*) Q and (*b*) C.

undeformed ferrite grains, the latter resulting from the deformed and subsequently transformed austenite (Figures 13g and h).

The textures of both specimens finished at 850 °C (schedules C and Q) show an austenite recrystallization texture (Figures 14a and b). Finishing at 800 °C, well within the intercritical range, shows a little higher intensity on the α-fiber and a slight overall reduction in intensity after coiling (Figures 14c and d). The sample rolled at 775 °C (Figure 14e) shows a more sharply defined ferrite deformation texture, whereas the coiled sample (Figure 14f), despite its remaining patches of deformed ferrite, looks very similar to the austenite recrystallization textures of Figure 14b, with a higher intensity on the H-component and along $\Phi = 0$. Finishing at 700 °C results in a sharp deformation texture, as already suggested by the microstructure, in both the quenched and coiled samples. The intensities of both textures are practically equal.

V. DISCUSSION

A. *Microstructure*

1. *Carbon steels: austenitic deformation*

The microstructures of the ELC and the LC steels after austenitic finishing, followed by a moderate cooling rate to the coiling temperature, are characterized by polygonal ferrite and pearlite grains. In comparison to the coiled samples, the only difference after quenching is a slight grain refinement as a result of the high cooling rate during quenching. The cooling rate was insufficient to induce formation of acicular ferrite in the ELC and LC steels. The CMn steel shows a ferrite-pearlite microstructure after coiling, whereas the sample after quenching shows areas with acicular ferrite or bainite grains. For the steels that were investigated, the cooling rate was insufficient for a complete transformation of austenite to martensite.

2. *Carbon steels: intercritical deformation*

A remarkable microstructural event is the occurrence of a bimodal distribution of grain sizes in the high-temperature intercritical region. The presence of the fine ferrite grain size could be attributed to the occurrence of dynamic recrystallization of ferrite. However, although the occurrence of dynamic recrystallization in ferrite has been reported in the literature,[20,21] it is generally believed that the likelihood of extensive dynamic recrystallization in ferrite at these high deformation temperatures and relatively low reductions is small and the recovery processes will prevail. Furthermore, dynamic recrystallization would result in a more gradual distribution of grain sizes, as this is a continuous process during deformation after a certain threshold strain has been overcome. The small grains have a narrow size range and are polygonal. A more detailed study of the microstructure, including local texture measurements using electron-backscattered diffraction, has revealed that the fine ferrite grains are actually subgrains.[22] The bimodal microstructure, therefore, consists of recrystallized ferrite and recovered ferrite.

The larger grains originate from deformed and recrystallized ferrite. To account for the large grain size, the recrystallization of the deformed ferrite has to proceed very rapidly. Since the recrystallization even occurs in the short time between finishing and quenching, which is a matter of seconds, the nucleation of the ferrite recrystallization has to be even faster. Usually, ferrite recrystallizes very slowly. The observed rapid nucleation indicates that the nucleation of the ferrite does not proceed along the lines of the SGC or SIBM mechanism, but by the transformation-induced (TI) nucleation mechanism.[23] Phase boundaries have been reported to act as efficient nucleation sites for further transformation.[24] The new ferrite grain nucleates at the austenite-ferrite phase boundary because the level of misfit is the highest there. The ferrite is then likely to grow into the deformed ferrite grains. The nucleus also grows into the deformed austenite, and since the nucleation takes place everywhere around the austenite grain, the austenite is consumed very rapidly. The ferrite nucleus that grows into the deformed ferrite consumes the deformed ferrite. The texture after recrystallization should provide some validation for this argument, since the transformed ferrite has an orientation relationship to the parent austenite as given by the Kurdjumov–Sachs orientation relation. The resulting large ferrite grains should also have that orientation if the nucleus generated by the TI mechanism has grown into the large grains. The probability of the TI mechanism occurring is enhanced by the fact that the large grain sizes only appear after a certain amount of transformation has occurred; in other words, when a sufficiently large fraction of deformed ferrite grains is present to be consumed by the TI nuclei. At lower austenite fractions during deformation, the TI nuclei grow until another nucleus is encountered. If the fraction of austenite is still large, the number of TI nuclei is high as well. The chance of impinging with a nucleus with another orientation is high, which will result in a cessation of grain growth for those particular grains.

Finishing the ELC steel at 825 °C followed by immediate quenching results in a microstructure consisting of a small fraction of unrecrystallized ferrite beside large recrystallized ferrite grains (Figure 4c). The time between rolling and quenching has obviously been too short to allow complete recrystallization, but too long to avoid recrytallization. The texture reveals that these grains originate from deformed and recrystallized ferrite (Figure 7c). The amount of unrecrystallized ferrite in the microstructure increases as the deformation temperature decreases. All deformation temperatures lead to a completely recrystallized microstructure after coiling. The grains on the α-fiber have a relatively low

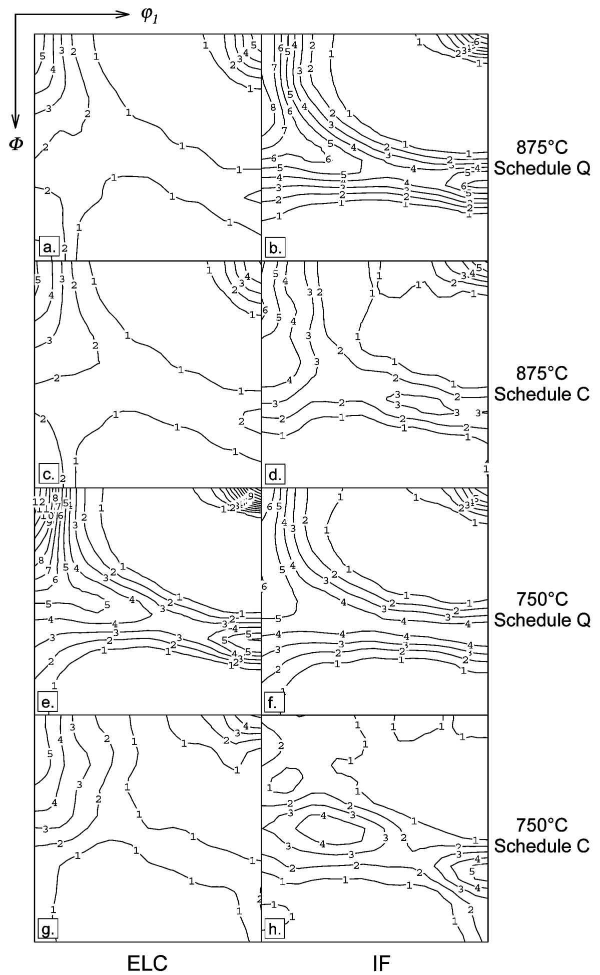

Fig. 11—Textures of the (*a*), (*c*), (*e*) and (*g*) ELC steel and (*b*), (*d*), (*f*), and (*h*) IF steel before and after coiling with a finishing temperature of (*a*) through (*d*) 875 °C and (*e*) through (*h*) 750 °C (e-h) (φ_2 = 45 deg section of the ODF, and intensity levels: 1, 2, 3, . . .).

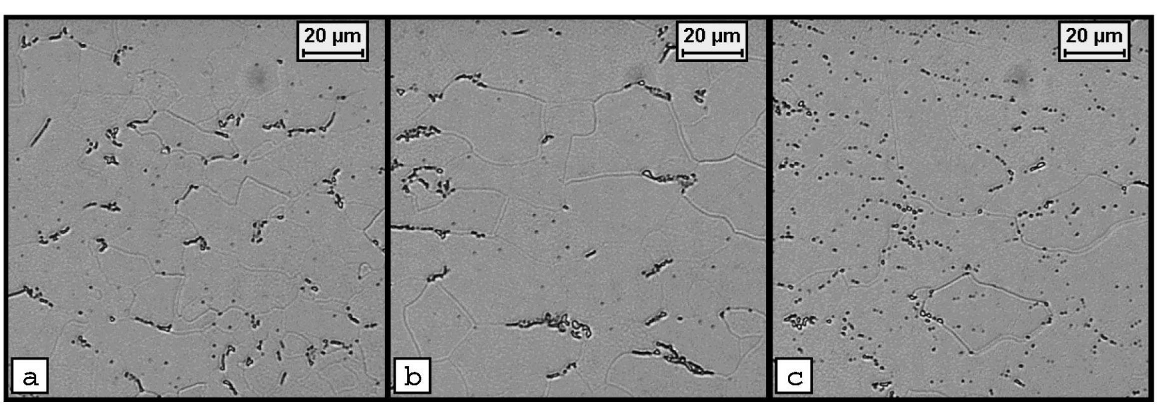

Fig. 12—Cementite morphology in LC steel (*a*) finished at 850 °C, (*b*) finished at 825 °C, and (*c*) finished at 700 °C (all schedule C).

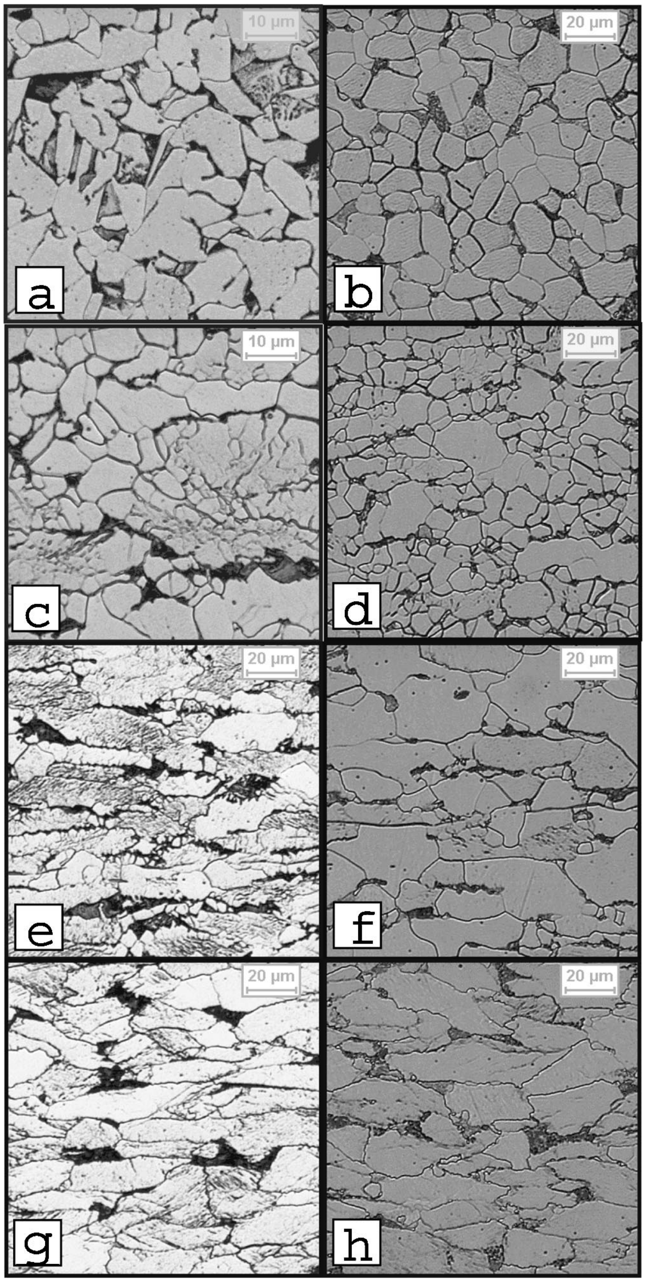

Fig. 13—Microstructures of CMn steel finished at 875 °C, schedules (*a*) Q and (*b*) C finished at 800 °C, schedules (*c*) Q and (*d*) C finished at 775 °C, schedules (*e*) Q and (*f*) C and finished at 700 °C, schedules (*g*) Q and (*h*) C.

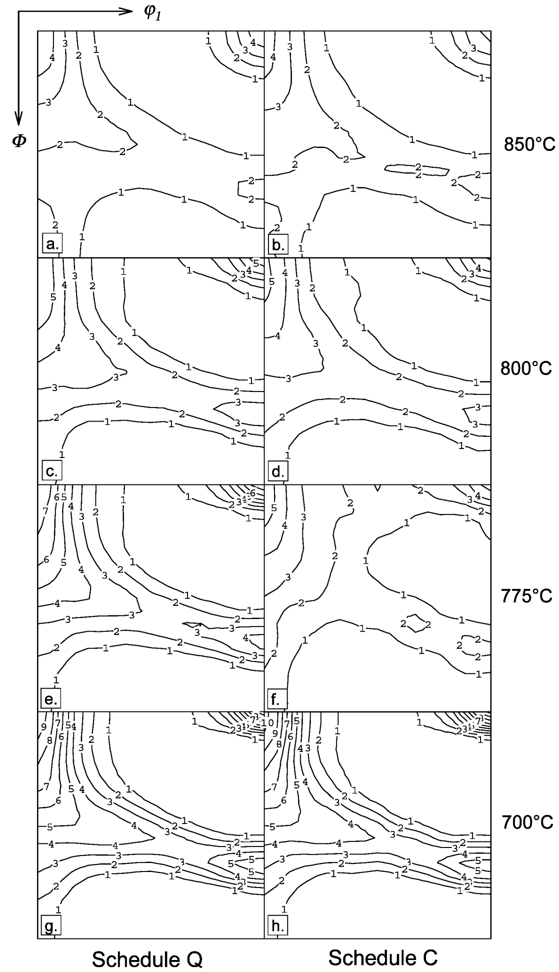

Fig. 14—Textures of the CMn steel before (schedule Q) and after (schedule C) coiling with a finishing temperature of (*a*) and (*b*) 850 °C, (*c*) and (*d*) 800 °C, (*e*) and (*f*) 775 °C, and (*g*) and (*h*) 700 °C (φ_2 = 45 deg section of the ODF, and intensity levels: 1, 2, 3, . . .).

stored deformation energy. In combination with the high recrystallization temperature, this will lead to nucleation by bulging of the deformed grain into a grain with a higher energy and, hence, will impose the low-energy orientation on this grain (SIBM). This means that the volume fraction of the low-energy component increases at the expense of the high-energy components.

3. *Carbon steels: ferritic deformation*

There is no essential difference between the fully ferritic rolling process (below 725 °C) and the low-temperature intercritical rolling process, as far as texture and microstructure are concerned. This suggests that the remaining fraction of austenite during intercritical rolling does not contribute to the texture any differently than the deformed ferrite, or that, if the influence does differ from the influence of ferrite, this contribution is too small to be observed. Because of the small amounts of austenite that are present during low-temperature intercritical rolling, the austenite grains will rotate to the stable orientation. After transformation to ferrite, this results in a component on or near T*, similar to deformed and SGC-nucleated ferrite grains, or in a component on the α-fiber.

Lower deformation temperatures in combination with the slow coil cooling (schedule C) do not lead to full recrystallization in the case of the CMn steel, even though the driving force for recrystallization is expected to be quite high, since the quenched microstructures are heavily strained. This can be explained by assuming that the relatively high aluminum content of this steel may lead to fine AlN precipitation at the coiling temperature of 650 °C. These precipitates can delay recrystallization.[17] Meanwhile, the dislocation density decreases due to recovery. If the recrystallization is inhibited long enough, the dislocation density can drop below the threshold to induce recrystallization by SIBM or SGC. Since there is (practically) no austenite left at a temperature of 725 °C or below, no ferrite nuclei can be formed by the TI mechanism.

4. *The IF steels*

The titanium content in the IF steel influences the recrystallization behavior of the austenite. This means that the texture and microstructure upon quenching from different temperatures according to the R schedule are no longer independent of the quenching temperature.

The coiled samples all recrystallized completely. A coiling temperature of 750 °C in combination with the final-pass deformation of 40 pct is obviously sufficient to induce complete recrystallization. The grain size of the ferritically or intercritically finished samples is much coarser (14 to 24 μm). From the quenched samples, it appears that after finishing at 875 °C or lower, the recrystallization of the sample occurs during the slow cooling, because none of the quenched samples show any trace of recrystallization. This difference in recrystallization behavior can be related to the absence of nucleation sites (in the form of remaining austenite-ferrite grain boundaries), in combination with very sluggish recrystallization of ferrite. The titanium contributes to the slow recrystallization by a solute-drag effect or a pinning effect by Ti precipitates.[19]

B. *Cementite Morphology in LC Steels*

In the LC material, the ferrite microstructure development is very similar to that of the ELC steel. The cementite morphology shows that deformation at 850 °C leads to cementite particles being oriented in all directions, whereas deformation at 825 °C causes the cementite to align in the rolling direction. At 850 °C, about 40 to 50 pct of the austenite is present. If the austenite is deformed, it recrystallizes and becomes polygonal again. After transformation, the cementite is polygonal as well (Figure 12a). At 825 °C, only 20 pct of the austenite is present. The deformed and, hence, elongated austenite grains are less likely to recrystallize into polygonal austenite grains at the lower finishing temperatures. Upon transformation, the elongated grains impose an elongated morphology on the cementite particles. After transformation of these “stretched” grains, the cementite remains in the same elongated form (Figure 12b). Deformation at 700 °C can be defined as fully ferritic finishing, and it causes either large recrystallized grains after coiling or heavily deformed ferrite grains after quenching. In the recrystallized structure, the cementite is distributed very finely through the microstructure along the former deformed ferrite grains or the present recrystallized ones. Some of the cementite that was already present before the last deformation is visible as stretched cementite clusters. In view of the moderate cooling rate before the final rolling pass, it seems reasonable to assume that most of the carbon had not yet precipitated before deformation. It precipitated as very fine cementite and, in view of the location of the cementite particles, preferably on the deformed ferrite grain boundaries. After recrystallization, these particles remain at these positions, thus marking the former ferrite grain boundaries (Figure 12c).

C. *Texture: Influence of Thermal Path Prior to and after Rolling*

1. *Schedule R: quenching prior to finish rolling*

The results indicate that cooling to the final rolling pass does not influence the texture development (schedule R in Figure 2) in the case of steels that do not contain any elements such as niobium or titanium, which affect the recrystallization behavior of the austenite. All samples show the maximum intensity in the $\varphi_2 = 45$ deg section at or near the H-component, the rotated cube texture, resulting from the recrystallization of austenite and subsequent transformation to ferrite. No relation was observed between either the quenching temperature and the intensity of the H-component within one steel grade, or the steel grade and intensity after quenching from the same temperature. The presence of the H-component obviously influences the texture development during further rolling (schedules Q, C, and AC) and is generally considered undesirable. However, in the absence of recrystallization-retarding elements in the austenite, little can be done to prevent the occurrence of the recrystallization texture. The IF grade shows a slightly different texture pattern because the remains of a deformation texture are visible (low intensities on or near the α-fiber (Figure 5)), indicating that the presence of titanium in the steel influences the recrystallization of the austenite. The presence of noncube-component intensities in the austenite results in non-H-components after the subsequent phase transformation. As the composition of the steel is not adequate to remove all interstitials *during* austenitic rolling, the different texture cannot be attributed to the absence of interstitials and must, therefore, be the result of retardation of recrystallization, caused by the addition of titanium. In all other steel grades, recrystallization-retarding elements were not present, resulting in largely the same behavior for all non-IF steel grades.

2. *Schedule AC: accelerated cooling after austenitic rolling*

From this study, it appears that the midthickness texture of the austenitically finished samples that underwent either accelerated cooling to the coiling temperature (AC) or slow air cooling to the same coiling temperature (C) is equal. All samples show a relatively strong H-component as well as a very weak intensity across a slightly tilted γ-fiber. Only the IF grade shows slightly higher intensities along the γ-fiber. In Figure 6, the intensity along the partial γ-fiber is shown for the ELC grade. The absence of a significant difference between the results of the samples produced according to the AC and the C schedules implies that the cooling rate in the range of 1 °C/s to 40 °C/s after austenitic finishing does not significantly influence the texture development. Since the microstructures indicate that the accelerated cooling does not lead to the formation of a different microstructure, but merely to a finer ferrite grain size in the case of the LC and CMn grades, this result is not surprising. In the IF and ELC steels, the grain size is not refined after accelerated cooling. Because of the similarity of the texture of the austenitically finished samples produced according to schedule C or Q (*i.e.*, slow cooling and coiling or quenching to room temperature, respectively), this leads to the conclusion that, within the processing parameters of this study, the cooling rate after austenitic finishing does not influence the final texture of the hot-rolled sample.

3. *Schedule Q: quenching after finishing*

a. *The ELC steel*

Intercritical rolling of the ELC steel at high temperatures causes an extension of the H-component along the α-fiber, and, from deformation temperatures of 775 °C and lower, a clear γ-fiber starts to develop. However, the intensity on the γ-fiber is never of the same magnitude as on the α-fiber. This is probably the result of the influence of the recrystallization texture that was inherited from the roughing passes. These passes result in a relatively strong austenite recrystallization texture. The intercritical pass will not completely erase this. In addition, deformation of the ferrite results in a strengthening of the α-fiber. The absence of the γ-fiber at high intercritical deformation temperatures is relevant because it is known that {111} grains nucleate from the preexisting {111} grains *via* the SGC nucleation mechanism. The absence of the {111} grains after finishing results in their absence after recrystallization and, consequently, in a texture that is less favorable for deep drawing.[10] After recrystallization, the intensity of the texture is not necessarily lower. In Figure 8b, the ratio of the volume fractions of grains on the α-fiber and the γ-fiber after coiling and quenching is plotted. This graph indicates that at finishing temperatures of 750 °C and lower, the volume fraction of grains on the γ-fiber after coiling (recrystallization) is much larger than after quenching, and that the volume fraction of grains on the α-fiber is not influenced by recrystallization. The relative increase of the γ-fiber with respect to the α-fiber, in combination with a general decrease of the intensities (see Figure 7), is indicative of a certain amount of randomization of the texture. Since the amount of carbon is too low to have cementite particles in the structure at this stage of the deformation, the randomization has to be explained otherwise. The TI nucleation is not very likely in view of the fact that the same phenomenon is only observed following deformation at 700 °C and lower.

Comparing schedule Q with schedule C for the components H, I, and E indicates that low finish rolling temperatures followed by coiling (recrystallization) lead to an increase of the volume fraction of all three components (Figure 8a). Since the total volume fraction of grains in the α-fiber does not change (Figure 8a), this means that there is a concentration of some orientations in the α-fiber. This indicates the occurrence of the SIBM mechanism. In this mechanism, the low-energy grains (*i.e.*, the ones on the α-fiber) tend to be preferential nucleation sites. Higher intercritical finish rolling temperatures (between 875 °C and 800 °C) lead to an increased volume fraction of the I component, but not to a change in the other orientations.

After finishing in the high-temperature intercritical region (between 875 °C and 800 °C), the maximum intensity is even higher in the recrystallized sample. In comparison to the austenitically rolled specimens, the texture increase along the cube fiber is notable (Figures 7b through h, top of the figure, along the $\Phi = 0$ axis). The γ-fiber is no longer present after finishing or after recrystallization. As explained earlier, there is a need for {111} grains to be present to be able to stimulate nucleation of new {111} grains.

Finish rolling in the ferrite region does not differ from the finishing in the low-temperature intercritical region. The intensities on the γ-fiber are high in the coiled samples, whereas they are low on the α-fiber. Before recrystallization, the intensities on the γ-fiber and the α-fiber are more or less equal.

b. *The IF steel*

Intercritical finishing reveals that finishing in the temperature range from 875 °C to 800 °C results in the highest intensity being on or very near the (0, 35, or 45 deg) orientations or the I component. This orientation is known to be a deformation-texture component and is the result of the transformation of the {112}⟨111⟩ austenite component followed by subsequent rotation as a result of the deformation of the ferrite (*cf.*, Table I). The intensity of the I component decreases steadily as the deformation temperature decreases. The decrease of the intensity is not the result of the lower deformation temperature *per se*, but the result of the decreased intensity of the {112}⟨111⟩ in the austenite. It is clear from this example that the inherited texture is, in some cases, more relevant to the final texture than the last deformation and the temperature at which it was performed. The clear maximum intensity on the deformation component disappears at lower deformation temperatures, leading to a flatter intensity distribution. In all cases, the γ-fiber is clearly visible next to the partial α-fiber, and this should lead to more favorable deep-drawing properties.

c. *The LC and CMn steels*

The texture development of the LC grade is very similar to the ELC grade. The largest difference is in the absolute values of the maximum intensities on the H-component, which are higher in the case of the LC steel. The CMn steel shows a similar behavior to the LC steel, albeit that as a result of the lower transformation temperatures, the increase as a result of the intercritical deformation has shifted to lower temperatures. The temperature region of intercritical deformation is noticeably smaller than for the LC steels.

4. *Schedule C: coiling after finish rolling*

a. *The IF steel*

In the textures of the intercritically rolled and coiled IF samples, two different features of the ODF can be distinguished in comparison to the ELC steel (compare Figures 11g and h). The ELC steel shows the highest intensities on the α-fiber, which suggests the SIBM nucleation mechanism for recrystallization. The IF steel shows the highest intensities near the γ-fiber (the T* component), which indicates the SGC nucleation mechanism for recrystallization. However, the maximum intensity on the T* component is low, with values of 5.

b. *The ELC and LC steels*

The textures of the intercritically finished and recrystallized samples all show results of the SIBM nucleation mechanism for recrystallization, with the higher intensities on the α-fiber and a nearly absent γ-fiber (shown for the ELC steel in Figures 11c and d).

c. *The CMn steel*

A significant difference between the CMn steel and the others is its sluggish recrystallization. Even in the sample finished at 775 °C and cooled according to schedule C, recrystallization is not complete (Figure 13f). This would suggest that the recrystallization temperature for the CMn steel is higher than that for the LC steel grade. This is not in agreement with practical experience during batch annealing after cold rolling. In that case, the temperature at which complete recrystallization is observed decreases with increasing carbon content, without showing intermediate minima. The incompletely recrystallized samples (775 °C and 750 °C) also show the effects of the SIBM nucleation mechanism for recrystallization in the resulting texture. This leads to the suggestion that, if the other samples would have recrystallized, the texture development would have been quite similar to the one observed in the LC steel. A detailed study of the microstructure and local texture, as well as of the state of precipitation of AlN, should be performed, because it is known that AlN influences and in some cases (temporarily) prevents the recrystallization behavior of low-carbon steels.[17]

D. *Calculated and Measured r_0 Values*

The r_0 value of the IF steel is considerably larger than for the other steels (Figure 9). This was already expected on the basis of the texture measurements. The best result corresponds with a calculated mean r-value of 1.4 and a Δr-value of 0.6. If we compare that to the results of an optimized chemistry and rolling schedule ($r = 1.7$ and $\Delta r = 0.9$), the present results are reasonable.[10] The differences between the calculated r_0 value and the experimentally observed r_0 value are significant, because the measured value also incorporates the effects of the surface shear components. The calculated value is based on the midthickness texture only. However, the trends of the calculated r_0 values reasonably follow the measured values.

The IF steel is the only steel with a change in sign of the Δr-value (Figure 9). Above 800 °C, the Δr-value is negative; below 800 °C, the Δr-value is positive. All other steel grades show a persistently negative value of the Δr-value.

VI. GENERAL OBSERVATIONS

A. *Microstructure: Recrystallization Nucleation and Grain Growth of Ferrite*

After deformation of single-phase austenite, the material will either recrystallize, generally to an austenite with a considerably finer grain size, or it will remain deformed until the transformation to ferrite starts. In the latter case, the deformed austenite will transform into very fine ferrite.[19] The first mechanism is used in the production of carbon-manganese structural steels, the second in the industrial production of high-strength, low-alloy steel sheet or plate.

In the case of intercritical deformation, the matter becomes complicated. If we consider an LC steel, it is safe to assume that the material before the final rolling pass has recrystallized and consists of austenite with (initially) small amounts of ferrite that nucleated at the austenite grain corners or grain boundaries. This two-phase structure is then deformed. The deformed austenite can either recrystallize, recover, or transform into a fine ferrite upon further cooling. The deformed ferrite does not recrystallize easily. The tendency to recover is much stronger than that for austenite. This leads to a sluggish nucleation of new ferrite grains from the deformed ferrite grains. The lack of ferrite nuclei explains the large grain size of the ferrite in a ferritically rolled product. However, if we consider the microstructure of the CMn steel rolled at 875 °C, 800 °C, and 775 °C, some remarkable features can be seen. First, rolling at 875 °C yields a fine ferrite with an average grain size of 8 μm (Figure 13b). Finishing at 825 °C, *i.e.*, well within the intercritical region (Figure 3), leads to an even finer grain size (6 μm), but the distribution starts to become bimodal. This is even more obvious after finishing at 800 °C (Figures 13c and d). Finishing at 775 °C, still within the intercritical region but with a much lower austenite fraction, unexpectedly leads to a mean ferrite grain size of 20 μm, together with an unrecrystallized ferrite fraction. A further decrease in rolling temperature results in an increase in the fraction of unrecrystallized ferrite. Finishing at 700 °C yields a completely unrecrystallized structure, even after a coiling simulation. The sudden increase in grain size in the high-temperature region (between 800 °C and 775 °C for CMn and between 850 °C and 825 °C for LC steel) was not observed for the ELC or IF steels. In these steels, the ferrite grain size increases as soon as the intercritical region is entered. Therefore, in the LC and CMn steels, a very noticeable microstructural event is the occurrence of a bimodal distribution in grain sizes in the high-temperature intercritical region. The explanation for this phenomenon was given in Section V–A–2.

As was also discussed in Section V–A–2, two main nucleation mechanisms are usually distinguished for the recrystallization of ferrite: the SGC mechanism and the SIBM mechanism. During intercritical rolling, a third nucleation mechanism for ferrite recrystallization may be active: the transformation of deformed or recrystallized austenite into ferrite. The transformed ferrite grains are strain free and have an orientation relation with the deformed austenite. Since these nuclei generally do not have a low-angle boundary with the deformed ferrite, the growth of these nuclei into the deformed ferrite will be very fast, resulting in large grains.

In the IF steel, where the intercritical deformation is not very important due to the limited size of the intercritical region, the large grains can be explained by the slow recrystallization of ferrite. From the microstructures of the quenched samples, it appears that this is the case. Samples rolled at 875 °C and lower show no sign of recrystallization, whereas the ELC steel rolled at 825 °C and subsequently quenched shows a large fraction of recrystallized grains. As a result of the slow nucleation from the deformed ferrite, the number of nuclei is low and a large grain size results.

B. *Influence of Carbon Composition on Microstructure and Texture*

The chemical composition influences the microstructure and texture development of the steels by affecting the equilibrium transformation temperatures. The elements in the steel may also influence the recrystallization behavior of deformed ferrite or austenite. In relation to intercritical deformation of LC steels, the chemical composition determines the nucleation mechanisms for recrystallization and, hence, the texture. A Ti-IF steel contains no cementite particles to randomize the microstructure during recrystallization in the coil. Furthermore, the presence of low concentrations of interstitials leads to higher volume fractions of high-energy grains with a favorable orientation.[7,25] In combination with a suitable annealing treatment, this should lead to a final product with an equally (or possibly even more) favorable orientation of the grains. The ELC steels do not have low concentrations of interstitials. This leads to lower intensities for the orientations on the γ-fiber and, because it recrystallizes at higher temperatures, to a higher tendency for the nucleation of ferrite from deformed ferrite according to the SIBM nucleation mechanism. During transformation of LC or CMn steels, cementite can form. If ferrite nucleates around these particles, the orientation of the ferrite will generally have no relation to that of the parent phase. On the other hand, in these steel grades, those ferrite grains nucleated as a result of the TI mechanism will have a clear orientation relationship to the parent phase.

VII. CONCLUSIONS

A series of trials has been performed on the laboratory pilot hot-rolling mill on an IF steel and three LC steels to investigate the development of microstructure and crystallographic texture during and after intercritical rolling. The finishing temperature was varied between 950 °C and 650 °C, and samples were taken just prior to the last finishing pass (schedule R), just after quenching following the last finishing pass (schedule Q), after being air cooled and coiled after the last finishing pass (schedule C), and after accelerated cooling and coiling (schedule AC). From this study, the following conclusions could be drawn.

1. Cooling of the samples to the entry temperature for the last rolling pass does not influence the texture of the sample. All samples show a high intensity on the H-component, resulting from the recrystallization of austenite and subsequent transformation to ferrite. There is no relation between the quenching temperature and the intensity of the H-component within one steel grade, or between the steel grade and intensity within one quenching temperature.
2. The midthickness texture of the austenitically finished samples cooled by either an accelerated cooling to the coiling temperature, or by a slow air cooling to the same coiling temperature, is equal. This implies that the cooling rate after austenitic finishing does not influence the texture development within the range of cooling rates in this study. Accelerated cooling after austenitic finishing may refine the ferrite microstructure, depending on the chemical composition.
3. Recrystallization after intercritical rolling leads to a decrease in texture intensity. In the case of recrystallization of ELC, LC, or CMn steels, the nucleation mechanism is an SIBM mechanism, which leads to unfavorable textures for deep-drawing applications. In the case of recrystallization of the IF grade after ferritic rolling, the nucleation mechanism shifts from the SIBM mechanism at high finishing temperatures to the SGC mechanism at low finishing temperatures. The latter mechanism leads to more favorable textures for deep-drawing applications.
4. Transformation-induced nucleation explains the occurrence of a sudden increase in ferrite grain size after high-temperature intercritical deformation of LC and CMn steels.
5. The calculated r_0 value for the ferritically rolled and quenched samples is at least equal to, but in most cases higher than, the value of the ferritically rolled and coiled samples. The only steel grade with a reasonable calculated mean r-value is the IF grade ($\bar{r} = 1.2$ to 1.4 with $\Delta r = 0.5$ to 0.6). The other grades all show low mean r-values of between 0.7 and 1.1. Δr-values are generally negative, with a mean value of about -0.4. In view of the texture data, there is a clear correlation between the occurrence of the SGC mechanism and higher r-values.

REFERENCES

1. R. Großterlinden, K.-P. Imlau, R. Kawalla, U. Lotter, and C.-P. Reip: *Steel Res.*, 1996, vol. 67, pp. 456-63.
2. R.K. Ray, M.P. Butrón-Guillen, J.J. Jonas, and G.E. Ruddle: *Iron Steel Inst. Jpn. Int.*, 1992, vol. 32 (2), pp. 203-12.
3. R.K. Ray and J.J. Jonas: *Int. Mater. Rev.*, 1990, vol. 35 (1), pp 1-36.
4. A. Akbarzadeh and J.J. Jonas: *Proc. 11th Int. Conf. on Textures of Materials (Icotom 11)*, 1996, pp. 683-88.
5. L. Kestens and J.J. Jonas: *Metall. Mater. Trans. A*, 1996, vol. 27A, pp. 155-64.
6. R.W.K. Honeycombe: *The Plastic Deformation of Metals*, 2nd ed., Edward Arnold (Publishers) Ltd., London, 1984.
7. R.K. Ray, J.J. Jonas, and R.E. Hook: *Int. Mater. Rev*, 1994, vol. 39, pp. 129-72.
8. *ISIJ International (Special Issue on Recent Advances in Modeling on Microstructural Evolution and Properties of Steels)*, N. Sano, ed., 1992, vol. 32 (3), pp. 261-449.
9. P. Van Houtte: *The "MTM-FHM" Software System, Version 2, Manual*, Katholieke Universiteit Leuven (B), 1995.
10. A. De Paepe, J.C. Herman, and V. Leroy: *Steel Res.*, 1997, vol. 68 (1), pp. 479-86.
11. M.P. Butrón-Guillen, C.S. Da Costa Viana, and J.J. Jonas: *Metall. Mater. Trans. A*, 1997, vol. 28A, pp. 1755-68.
12. K. Lücke and J. Hirsch: *in Directional Properties of Materials*, H.J. Bunge, ed., DGM Informationsgesellschaft Verlag, Oberursel, 1988, pp. 85-101.
13. H. Inagaki: *Z. Metallkd.*, 1984, vol. 75, pp. 510-16.
14. H. Inagaki: *Z. Metallkd.*, 1988, vol. 79, pp. 716-23.
15. I.L. Dillamore, C.J.E. Smith, and T.W. Watson: *Met. Sci. J.*, 1967, vol. 1, pp. 49-54.
16. M. Onink: Internal Report No, 89722, Corus Research, Development & Technology, 1998.
17. W.B. Hutchinson: *Int. Met. Rev.*, 1984, vol. 29, pp. 25-42.
18. A. Van Bael, J. Winters, and P. Van Houtte: *Proc. 11th Int. Conf. on Textures of Materials (Icotom 11)*, 1996, International Academic Publishers, Beijing, pp. 356-61.
19. I. Tamura, H. Sekine, T. Tanaka, and C. Ouchi: *Thermomechanical Processing of High-Strength Low-Alloy Steels*, Butterworth and Co., London, 1988.
20. G. Glover and C.M. Sellars: *Metall. Trans.*, 1972, vol. 3, pp. 2271-80.
21. G. Glover and C.M. Sellars: *Metall. Trans.*, 1973, vol. 4, pp. 765-75.
22. A. Bodin, J. Sietsma, and S. van der Zwaag: *Mater. Characterization*, 47/3-4, 2002, pp. 187-93.
23. D. Vanderschueren, L. Kestens, P. Van Houtte, E. Aernoudt, J. Dilewijns, and U. Meers: *Mater. Sci. Technol.*, 1990, vol. 6, pp. 1247-50.
24. M.R. Barnett and J.J. Jonas: *Iron Steel Inst. Jpn. Int.*, 1999, vol. 39 (9), pp. 856-73.
25. K. Eloot, J. Penning, and J. Dilewijns: *Steel Res.*, 1997, vol. 68, pp. 450-56.